Tight-binding molecular dynamics simulations of radiation-induced C_{60} fragmentation

Titus A. Beu,* Lóránd Horváth, and Ioan Ghişoiu
Faculty of Physics, University Babeş-Bolyai, 400084 Cluj-Napoca, Romania
(Received 12 October 2008; published 26 February 2009)

The radiation-induced fragmentation of the C_{60} fullerene was investigated by tight-binding molecular dynamics simulations based on the parametrization of Papaconstantopoulos *et al.* [*Tight-Binding Approach to Computational Materials Science*, edited by P.E.A. Turchi, A. Gonis, and L. Colombo, M.R.S. Symposia Proceedings No. 491 (Materials Research Society, Pittsburgh, 1998), p. 221] and employing novel models for nonadiabatic excitation and charge redistribution. The resulted fragment size and fragment charge distributions, averaged over large ensembles of trajectories corresponding to total ionization states up to $+24e$ and excitation energies up to 1000 eV, have been used to analyze the fragmentation statistics in terms of several derived quantities. For moderate excitation energies, the fragment size profiles reproduce the experimentally observed U shape and bimodal dependence. Even though for high excitation energies and high total charges, predominantly multifragmentation occurs, a genuine power-law dependence sets in only beyond 1000 eV. A well-defined phase-transition region is found in the total charge-excitation energy plane, which appears to be delimited by a roughly parabolic critical line. The overall average critical excitation energy estimated from the simulations amounts to 55 eV and agrees with the experimental findings.

DOI: 10.1103/PhysRevB.79.054112 PACS number(s): 71.15.Mb, 71.20.Tx

I. INTRODUCTION

Fullerenes can undergo a wide variety of processes ranging from charge transfer and ionization to atom capture, fusion, and fragmentation, depending on the type of the used projectiles (photons, electrons, ions, fullerenes, etc.) and their impact energy and electrostatic charge.[1,2] In the abundance of experimental evidence on collision-induced fullerene dissociation, usually acquired from time-of-flight (TOF) spectrometers,[1] a plethora of processes have been found, among which evaporation (cleavage) of light even numbered C_{2n} clusters, fission into heavy and light (neutral or charged) fragments, much smaller than C_{60}, and multifragmentation into several light fragments have been more intensely studied.[2–4]

While the first systematic study of radiation-induced fullerene fragmentation was done by O'Brien *et al.*[5] using nanosecond laser pulses, more recent experiments, tackling the process by means of femtosecond laser ablation,[6–12] and also a few newer computer simulations[13–15] give more insights into the specific dynamics of C_{60} dissociation.

During laser-induced fragmentation, the fullerene undergoes complex electron transfer processes, among which ionization plays the most important role. Concerning the ionization mechanism of C_{60} in femtosecond laser pulses, there are rather diverging opinions in the literature.[9] For instance, the pathway responsible for ionization of C_{60} was considered by Hunsche *et al.*[10] to be the excitation of a giant resonance near 20 eV, while, more recently, Tchaplyguine *et al.*[7] brought forward arguments in favor of the direct multiphoton ionization. Anyway, ionization processes during fragmentation dynamics of C_{60} irradiated with intense femtosecond laser pulses are found to vary to a large extent, depending on the intensity and duration of the laser pulse.

In the first report on ion-induced fragmentation of fullerenes,[16] the collision-induced dissociation reactions of mass-selected C_{60}^+ and C_{70}^+ at laboratory collision energies in the range 5–8 keV were investigated. Fragmentation mass spectra down to C_{40}^+ were reported with peaks separated by 24 amu (corresponding to successive C_2 evaporations). Interestingly, the mass spectra were very similar to those reported earlier by O'Brien *et al.*[5] for the photodissociation of mass-selected fullerenes. A number of other groups have since reported related results using a variety of larger gaseous targets.[17–19] In these experiments, for sufficiently high excitation energies a *bimodal* fragmentation pattern was observed, consisting of large even-sized fragments $C_{2n}^+(n>16)$ and small clusters $C_n^+(n<32)$. Another common characteristic of these experiments is that the electronic system is excited on a short-time scale (5–100 fs) (Refs. 1, 3, 8, and 12) as compared to the electron-phonon coupling time ($\sim$250 fs).[20]

The deposited threshold energy for the C_2 evaporation was determined experimentally by Rentenier *et al.*[3] to lie around 50 eV, while the elementary C_2 dissociation energy from C_{60}, calculated by Boese and Scuseria[14] by means of perturbative quantum chemical methods, was predicted above 10 eV.

Since extensive density-functional theory based molecular dynamics (MD) simulations of electronic, energetic, and vibrational properties of large carbon nanostructures (such as fullerene polymers or carbon nanotubes) are still beyond the capabilities of state-of-the-art computers, there is an obvious need for less time consuming methods, which however preserve a good level of accuracy. It is well known that tight-binding molecular dynamics (TBMD) schemes meet these requirements and are therefore widely used.[13–15,21–28]

Over the last years, we have successfully employed the tight-binding (TB) parametrization scheme of Papaconstantopoulos *et al.*[29] in simulations of structural and vibrational properties of a variety of fullerenes (C_{36}, C_{60}, and C_{70}) and of their polymers.[21–24] Quite recently, we have applied it also in the investigation of the laser-induced fragmentation of fullerenes.[25]

The majority of C_{60} fragmentation experiments, irrespective of the excitation mechanism (laser, electron or ion beam, etc.), typically report the evaporation of *charged* species,[3,8,12] a significant detail which is usually overlooked in TB studies. This also applied to our previous work,[25] which was based on the simple assumption that C_{60} breaks apart into noncharged fragments. The neglect of the electron-phonon coupling, on the other hand, should be less crucial since, as already pointed out, the short energy-deposition times found in experiments should minimize such coupling effects.[20]

The present paper reports results of simulations of radiation-induced C_{60} fragmentation performed by means of the above mentioned TBMD scheme.[29] Our calculations consider charged fragments and employ explicit excitation and charge redistribution models. Even though TBMD studies are not particularly innovative in their own right, rather phenomenological results can be found in the literature so far. From this perspective, our present approach should offer a deeper, quantitative insight into the fragmentation dynamics.

II. SIMULATION DETAILS

TB approaches can be viewed as simplified two-center-oriented *ab initio* methods, with the electronic properties calculated from a parametrized representation of the Kohn-Sham equation. The TB parametrization of Papaconstantopoulos *et al.*[29] describes the environment of each atom by a pseudoatomic density

$$\rho_I = \sum_{J \neq I}^{N} \exp(-\lambda^2 R_{IJ}) f(R_{IJ}),$$

which depends exponentially on the distances to all neighbors and features a cutoff function, $f(R) = \{1 + \exp[(R - R_c)/\Delta]\}^{-1}$, implying specific parameters for carbon ($R_c = 10.5a_0$ and $\Delta = 0.5a_0$).

The specific structure of the Hamiltonian equations yielding the one-electron energies has been described in detail in our previous publications.[21–25] The (diagonal) *on-site* Hamiltonian elements are parametrized in terms of the local pseudoatomic density ($l = s, p$),

$$h_l^I = \alpha_l + \beta_l \rho_I^{2/3} + \gamma_l \rho_I^{4/3} + \chi_l \rho_I^2.$$

The two-center Slater-Koster hopping terms involved in the construction of the 4×4 off-diagonal blocks of the Hamiltonian and overlap matrices are defined as polynomials with an exponential cutoff ($\mu = \sigma, \pi$),

$$H_{ll'\mu}(R) = (a_{ll'\mu} + b_{ll'\mu} R + c_{ll'\mu} R^2) \exp(-d_{ll'\mu}^2 R) f(R),$$

$$S_{ll'\mu}(R) = (\delta_{ll'} + p_{ll'\mu} R + q_{ll'\mu} R^2 + r_{ll'\mu} R^3) \times \exp(-s_{ll'\mu}^2 R) f(R).$$

This TB parametrization accounts essentially for the four tightly bound valence electrons of each carbon atom, maintaining the system and the resulted fragments electrically neutral.[25] Since the explicit inclusion of ionization in this scheme would assume a very complex overall reparametrization, charged states will be considered by means of a separate model described in the following.

The lack of an adequate model accounting for electronic excitation (including ionization) was a drawback of our previous work.[25] In the present investigation our approach is significantly improved by explicitly considering positively ionized fragments produced along the trajectories by simple electronic ionization processes. Anyway, the simulated fragment size distributions are expected to differ slightly from the experimental ones yielded by TOF spectrometers, since the latter are inherently averaged both over electrically neutral and charged fragments. On the other hand, the huge diversity of experimental setups makes it difficult for one to develop a universally applicable model.

In generic fragmentation experiments, the particular final ionization states of the fragments clearly result from the whole fragmentation history, varying for different trajectories. A single trajectory traces all configurations from the actual excitation of the fullerene to the detection of the fragments and, as an illustration, snapshots from one particular fragmentation trajectory are depicted in Fig. 1. In our simulations we have considered separate ensembles of trajectories corresponding to fixed total charges (final cumulated ionization states of the fragments) and particular excitation energies. Specifically, all measurements have been performed in terms of these two main parameters: the *total charge* and the *excitation energy*. The latter can be related to the so-called deposited energy, a quantity often referred to in experimental fragmentation studies.[1,3] System states featuring total charges up to $+24e$ and excitation energies between 0 and 1000 eV have been dealt with, with a view to elucidate the dependence of the fragmentation statistics on these parameters. In terms of total binding energy of the C_{60} cage (defined as difference between 60 times the individual atomic energy and the total tight-binding energy), the upper limit of the excitation energy reaches approximately $1.66E_{\text{bind}}$.

The initial equilibrium configuration of the fullerene cage employed here is the one used in our previous investigations[25] and it was generated by simulated annealing embedded in the outlined TB molecular dynamics framework.[21] Bond lengths (1.41 and 1.44 Å, respectively) were found to be in error by less than 2.5% with respect to experimental NMR data and density-functional calculations,[28,30] and the highest occupied molecular orbital–lowest unoccupied molecular orbital (HOMO-LUMO) gap (1.71 eV) fits also fairly in the experimental range (1.6–1.85 eV).[31] For each given pair of parameters (total charge, excitation energy), an ensemble of 200 C_{60} cages have been fragmented and ensemble-averaged fragmentation statistics was subsequently performed.

In order to develop a good understanding of the fragmentation mechanism, we also placed emphasis on realistically modeling the initial excitation of the system. For fullerene fragmentation, the vast majority of experiments uses laser pulses ranging from a few to several hundreds of femtoseconds.[6,8,9,11,12] As an improvement over our previous work,[25] where the cage was excited adiabatically, the current study employs a ramplike input of both excitation energy and charge. Specifically, with a view to discern the relevance of the details of the excitation mechanism, in addition to the

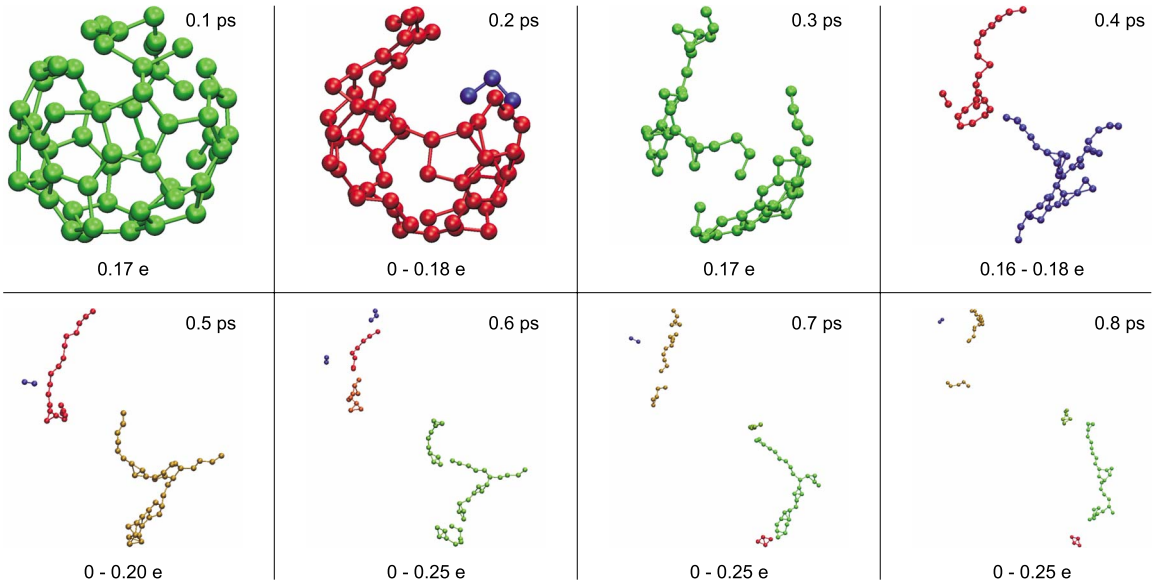

FIG. 1. (Color online) Snapshots at time intervals of 0.1 ps from a fragmentation trajectory corresponding to a total ionization charge $q=+10e$ and an excitation energy of 100 eV. The range between the lowest and the highest fragment charge is represented for each snapshot by the color scale blue-green-red (light to dark).

adiabatic excitation, we have comparatively considered excitation ramp durations of 0.1 and 0.5 ps, respectively.

As part of the actual heating mechanism, the atoms acquire different random velocity patterns at the beginning of each trajectory. Concretely, at each time step of the excitation ramp, the system receives equal elementary excitations, involving small random corrections applied to the atomic velocities, which sum up eventually to the aimed total excitation energy.

An analogous mechanism is used also for ionization, an integer charge (less or equal to the total charge) being added periodically (at equal number of steps). If the aimed total charge exceeds in absolute value the number of steps assigned to the excitation ramp, several elementary charges are added at each excitation step (in the limiting adiabatic case, the system acquires the total charge from the very beginning). If the fullerene fragments during the excitation ramp, the charge to be added is placed on a random fragment.

The charge (ionization state) of any fragment should be, obviously, an integer. However, individual atoms can be assigned also fractional charges within the fragments, resulting from the ratio of the integer fragment charge to the number of contained atoms. In particular, we calculate the electrostatic interactions by using the partial atomic charges and the corresponding spatial positions. In any case, a charge redistribution algorithm needs to be applied whenever the fragment size distribution changes, the underlying idea being to produce step-wise changes of the fragment charges reflecting the relative electron localization emphasized also by other authors.[8]

In our basic model, any new fragment is assigned in the first instance the sum of the partial charges carried by the composing atoms in their originating fragments. The fragments, which can thus have initially a fractional charge, are then ordered increasingly according to their deficit to the next-higher integer charge. The cumulated fractional charge exceeding the integer charges of all fragments, which is always an integer, is then redistributed (until exhaustion) to the new fragments in increasing order of their charge deficit, such as to round their charges up, while for the fragments with higher deficit the charge is eventually rounded down. By this redistribution scheme, the total ionization state is conserved and the jumps in the fragment charges are minimized. As another natural consequence, due to the incidental transfer of integer charges among newly formed fragments, the electrostatic energy may exhibit fluctuations (reflected also in the total energy) along the trajectory.

As an alternative to the above charge redistribution algorithm, we have also examined a second model of extreme simplicity, in which the partial atomic charges are kept constant and equal to the ratio of the total charge of the fullerene to the total number of atoms. Of course, in such a model also fragments with fractional charges can occur. Quite surprisingly, however, despite its apparently reduced physical contents, this uniform atomic charge assignment model gives comparable results to the ones obtained with the more elaborate redistribution algorithm, altering by less than 0.5% the fragmentation probability under similar conditions. This can be readily understood by regarding the fractional fragment charge distributions as time-averages over distributions of integer fragment charges.

Each fragmentation trajectory is propagated using a constant time step, which depends exponentially on the particular excitation energy, specifically, decreasing from 0.5 fs for 100 eV to 0.05 fs for 500 eV. For example, when applied in conjunction with the simple model of uniform atomic charges, this exponential dependence insures a relative accuracy of 10^{-3} in the total energy. The fragments are identified by the recursive labeling algorithm used also in our previous work, as part of which each atom is labeled by the index of the fragment it belongs to.

The termination of a trajectory is decided by verifying two stopping criteria every 1000 time steps, the first time

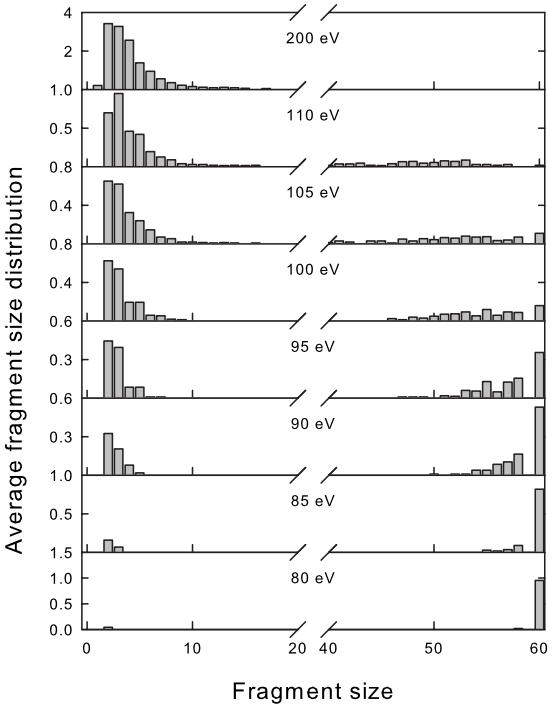

FIG. 2. Ensemble-averaged fragment size distributions of neutral fragments for different excitation energies.

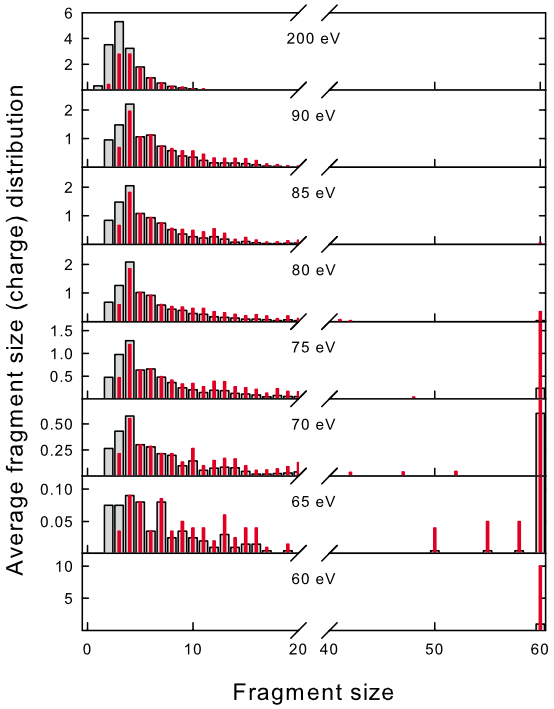

FIG. 3. (Color online) Ensemble-averaged fragment size and charge (with red) distributions for total charge +10*e* and different excitation energies.

after 3000 steps. The first termination criterion is fulfilled if between two consecutive checkpoints the fragment size distribution remains unchanged, or technically, if the labels of atoms did not change. The second termination criterion, which is more stringent, is fulfilled if the distance between any two fragments is larger than the extent of the tight-binding C-C potential well (~4 Å), which renders the recombination probability negligible.

III. RESULTS AND DISCUSSION

The primary quantities monitored in our simulations are the fragment size distribution and the fragment charge distribution. They have been recorded for each combination of total charge and excitation energy as averages over ensembles of 200 trajectories. All other quantities of interest are derived from these two ensemble-averaged distributions and they will be detailed in the following. The actual values considered in the simulations for the total charges have been $q_{\mathrm{tot}}=0-24e$ and for the excitation energies $E_{\mathrm{exc}}=0-120,150,200,500,1000$ eV (sampled equidistantly up to 120 eV at intervals of 5 eV). As central quantities of interest, the fragment size distribution and the fragment charge distributions are presented comparatively in Figs. 2–4 for three illustrative total charges ($q_{\mathrm{tot}}=0,10e,20e$) and several excitation energies.

As can be seen in Fig. 2, the ionizationless fragmentation of C_{60} (leading solely to neutral fragments) sets in around 80 eV and the gradual shift of the distribution maximum to smaller clusters with increasing excitation energy is apparent. The U shape of the size distribution (with absent C monomers), evidenced also experimentally by Rentenier *et al.*,[3] is noticeable at intermediate energies (between 90 and 110 eV). Furthermore, a bimodal size dependence appears to characterize predominantly the large fragments, in agreement with other calculations from the literature.[7,13] The C_2 dimer

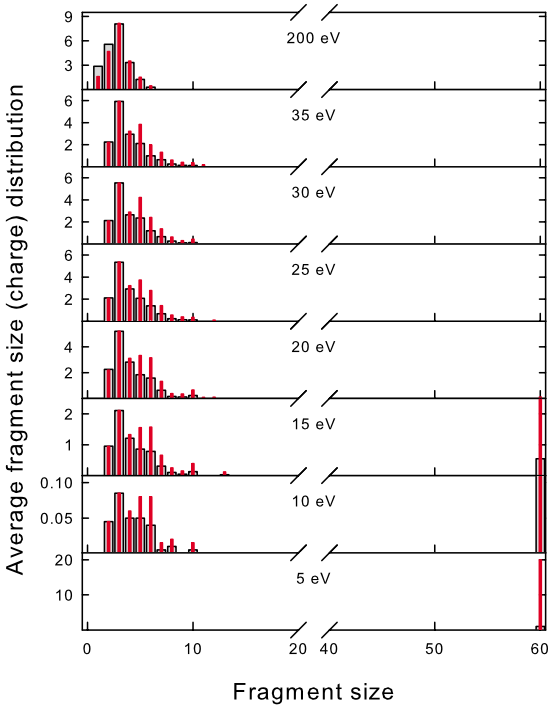

FIG. 4. (Color online) Ensemble-averaged fragment size and charge (with red) distributions for total charge +20*e* and different excitation energies.

cleavage leading to bimodal fragmentation patterns was studied extensively[1,3,32–34] and we have discussed it in detail previously.[25] Hence, we will not address it to a greater extent.

The distribution patterns appear to be also similar to those from a wide variety of fragmentation experiments involving atomic projectiles.[3,32,35,36] Moreover, the C_{60} melting temperature we have obtained for the chargeless fragmentation ($\sim$5700 K) is in agreement with the qualitative result (5400 K) of the simulations of fullerene melting performed by Kim and co-workers[26,27] by using a simpler tight-binding approach.

The size distribution obtained at 500 eV for chargeless fragmentation (not shown) prefigures the transition to a power law, which becomes obvious for energies higher than 1000 eV. The excitation energy being on average equally distributed between translational and rotational degrees of freedom, roughly twice the molecular binding energy ($\sim$1200 eV), would be required to fully dissociate the neutral fullerene. However, our simulations show that even for excitation energies way beyond 1000 eV, due to the substantial kinetic energy acquired by the fragments, besides monomers, albeit rarely, carbon dimers still remain discernible at the end of the trajectories.

For the two ionization states illustrated in Figs. 3 and 4 ($q_{\mathrm{tot}}=10e$ and $20e$), the fragmentation can be seen to set in at 65 and 10 eV, respectively. Despite the overall shift of the fragmentation profiles to smaller sizes with increasing total charge, U-shape distributions are no longer observable as in the neutral case and this is due to the strong Coulomb repulsion within the large fragments, which leads to their successive disintegration into smaller ones.

The average charge distributions, specifying the average charge on *all* fragments of a given size, behave at first glance similarly to the fragment size distributions and they are plotted in Figs. 3 and 4 as thin red vertical lines, superimposed over the size distributions. If needed, the average charge on a fragment of given size can be easily obtained by dividing the charge and size distributions. By analyzing the profiles for $q_{\mathrm{tot}}=10e$ (Fig. 3), one can notice that the charge distributions are shifted slightly relatively to the size distributions toward larger sizes (roughly by one size unit). This indicates that a moderate total charge is preferentially accommodated by larger fragments and this is readily understandable, since this arrangement reduces the electrostatic interactions. In the case of the higher total charge, $q_{\mathrm{tot}}=20e$ (Fig. 4), the charge profiles appear to follow closely the size profiles, since the charge fills up the fragments as uniformly as possible. Noteworthy, the larger the total charge, the more the results appear to be similar to those yielded by the simpler uniform atomic charge assignment model we have tested.

By contrast to the *quantitative* representation given by the *number* size distributions plotted in Figs. 2–4, the trajectory snapshots shown in Fig. 1 are intended to give solely a *qualitative* idea of the actual *geometrical* fragment sizes. For each trajectory ensemble considered, the distributions of geometrical features (for example, the gyration radius) have been inherently affected by substantially larger fluctuations than the corresponding number size distributions and they will not be discussed further.

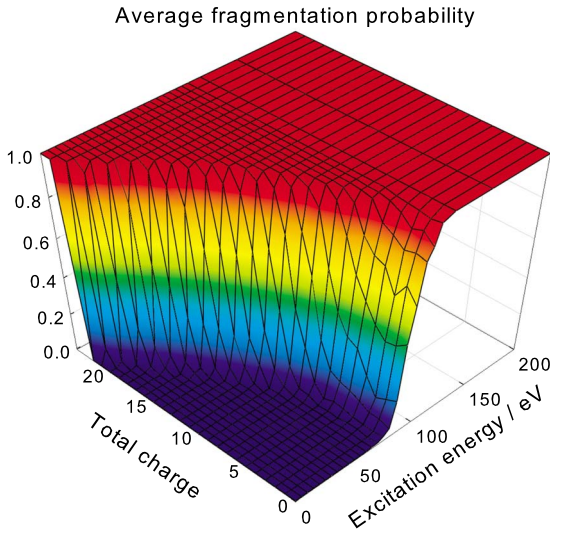

FIG. 5. (Color online) Average fragmentation probability as a function of total charge and excitation energy.

The average fragmentation probability, providing the most synthetic description of the overall features of the fragmentation process, is defined straightforwardly for each trajectory ensemble (corresponding to a given total charge-excitation energy combination) by the ratio of the number of dissociated cages to the total number of trajectories. Figure 5 shows the three-dimensional plot of the fragmentation probability as a function of the total ionization state and excitation energy. Between the (red) plateau corresponding to certain fragmentation for each trajectory (certain-fragmentation region) and the (blue) valley corresponding to the total absence of fragmentation (nonfragmentation region), a well-defined transition region with a monotonous and abrupt increase with respect to both parameters is visible. As can be readily noticed, the two-dimensional (2D) cross sections for fixed total charge become steeper functions of the excitation energy, while the nonfragmenting region becomes narrower with increasing total charge.

Defining the critical (threshold) excitation energy for a given total charge as the input energy corresponding to an average fragmentation probability of 0.5, the threshold is found for chargeless fragmentation around 90 eV, as already reported in our previous work[25] and in agreement with earlier simulations.[26,27] The critical excitation energy decreases roughly quadratically with respect to the total ionization state (as will be discussed later on and shown in Fig. 14), such that a total charge value ($q_{\mathrm{tot}}\simeq 24e$) is eventually reached, for which the fragmentation occurs without any energy input.

One of our aims was also to assess the relevance of different aspects of the employed ramplike excitation model and, in this regard, we studied the influence of the excitation duration. Figure 6 illustrates the fragmentation probability profiles for combinations of three different total charges ($q_{\mathrm{tot}}=0,10e,20e$) and three different excitation times ($t_{\mathrm{exc}}=0,0.1,0.5$ ps). As expected, the instantaneous excitation is the most effective in terms of fragmentation probability and with increasing excitation time the transition region shifts toward higher energies, indicating that fragmentation becomes less probable. Equally, the differences induced by dif-

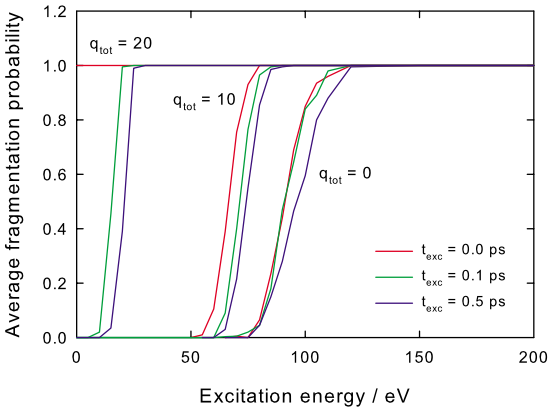

FIG. 6. (Color online) Average fragmentation probability as a function of the excitation energy for selected total charges ($q_{\mathrm{tot}}=0,10e,20e$) and excitation times ($t_{\mathrm{exc}}=0,0.1,0.5$ ps).

ferent excitation times are found to increase with increasing total charge. Whenever not specifically mentioned otherwise, the presented results pertain to the excitation ramp duration of 0.1 ps, which is our reference prescription.

Figure 7 displays the (up to statistical fluctuations) monotonically increasing profiles of the average number of fragments as functions of the excitation energy for the three total charges and three excitation times invoked above. In the transition region the slopes increase considerably with increasing total charge indicating high instabilities in the system. In the higher energy region, the average number of fragments appears to depend roughly linearly on the excitation energy and quadratically on the total ionization state.

Different excitation times affect the average number of fragments in a fairly similar manner with the case of the average fragmentation probability: the instantaneous excitation increases, while longer excitation times lower the average number of fragments produced along a trajectory. Since the average number of fragments tends naturally to the total number of atoms with increasing excitation time and/or total charge, its dependence is not linear in the high energy range, as it may appear. In addition, higher total charges augment the differences induced in the profiles by the different excitation times. The highest effectiveness of the adiabatic excitation can be traced back again (as in the case of the fragmentation probability) to the ramplike excitation mechanism, where, for finite excitation times, the successive velocity corrections are added to already partially correlated atomic velocities, rendering fragmentation less probable.

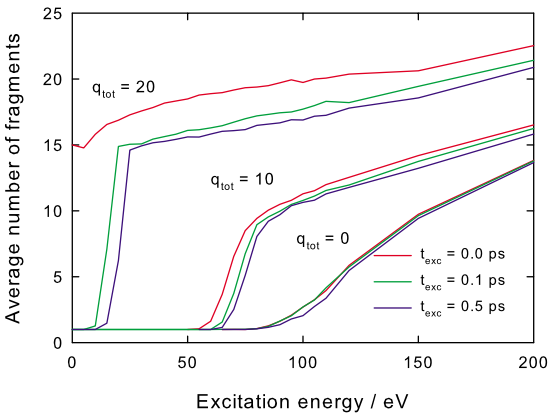

FIG. 7. (Color online) Average number of fragments as a function of the excitation energy for selected total charges ($q_{\mathrm{tot}}=0,10e,20e$) and excitation times ($t_{\mathrm{exc}}=0,0.1,0.5$ ps).

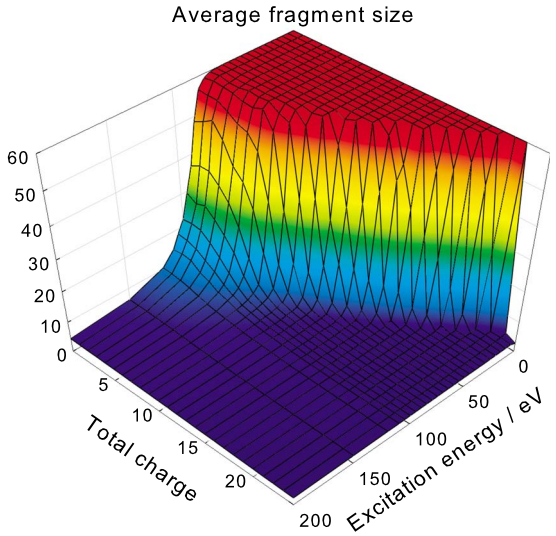

FIG. 8. (Color online) Average fragment size as a function of total charge and excitation energy.

Another illustrative quantity derived from our simulations has been the average fragment size (Fig. 8), calculated for each combination of total charge and excitation energy as average of the ensemble-averaged fragment size distribution. From the total number of atoms in the nonfragmenting region, it decreases abruptly in the transition region toward small values with respect to both parameters, tending asymptotically to the limiting value 1 (complete fragmentation). This quantity is complementary to the average number of fragments and their product should be within statistical errors constant and equal to the total number of atoms, namely, 60. Indeed, the maximum relative error of the computed product was found to be 0.3%, proving that the ensembles of 200 trajectories considered provide reasonably good statistics.

The average maximum fragment size (Fig. 9), as maximum of the ensemble-averaged fragment size distribution, follows qualitatively the behavior of the average fragment size, featuring, nevertheless, a rupture around the nonfragmenting region, a less steep decrease and a moderate noise in the transition region. As for the average minimum fragment size (not shown), it is characterized by a very abrupt drop in the transition region and quite appreciable noise in the fragmentation region due to the occasional occurrence of monomers along dimers for trajectories corresponding to high total ionization states and/or excitation energies.

In order to understand the charge distribution at the end of the fragmentation process, we have also investigated, similarly to the average fragment size, the average fragment charge. As one would expect, this quantity increases linearly with the total charge in the nonfragmenting region (see Fig. 10) and drops sharply in the transition region toward an al-

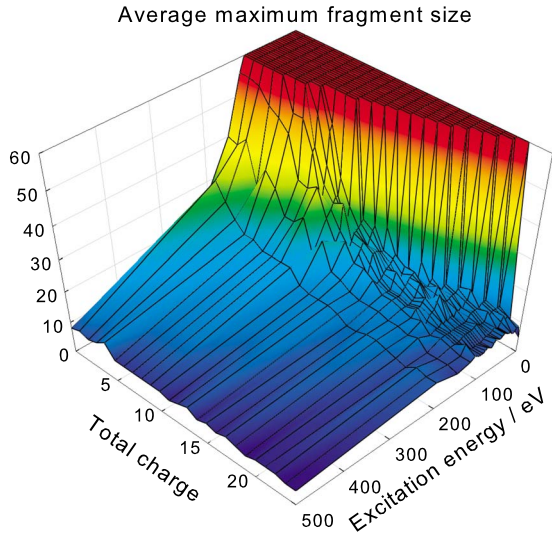

FIG. 9. (Color online) Average maximum fragment size as a function of total charge and excitation energy.

most flat plateau with a smooth decline with respect to energy and a slow increase with respect to charge. Another suggestive analysis can be undertaken in terms of a normalized average fragment charge, defined as the average fragment charge divided by the total charge characterizing the ensemble. This dependence is absolutely analogous to that of the average fragment size (Fig. 8), however decreasing abruptly from 1 in the nonfragmenting region and reaching asymptotically (for large total charges and/or large excitation energies) a value equal to the ratio of the total charge to the total number of atoms (complete fragmentation down to monomers).

A similar relation as between the average number of fragments and the average fragment size also exists between the average number of fragments and the average fragment charge. Specifically, their product should equal the total charge. Indeed, we find this relation to hold up to a maximum relative error of 0.5%, proving again the fair statistics provided by the employed trajectory ensembles.

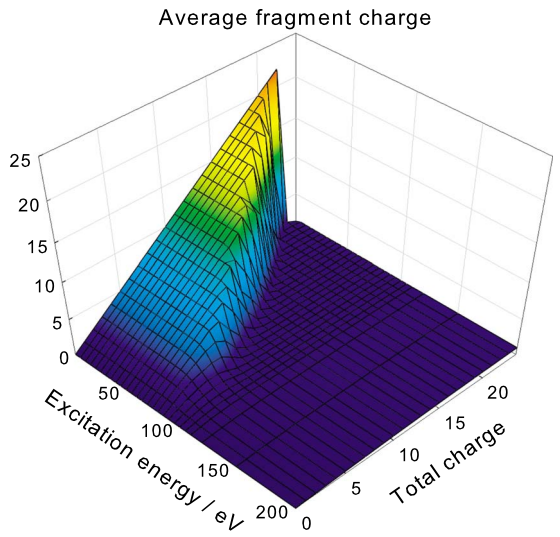

FIG. 10. (Color online) Average fragment charge as a function of total charge and excitation energy.

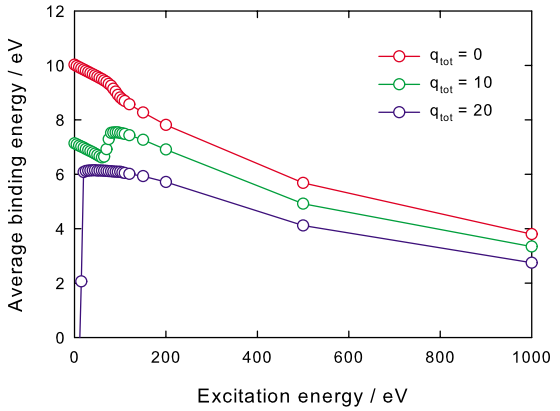

FIG. 11. (Color online) Average binding energy as a function of the excitation energy for selected total charges ($q_{\mathrm{tot}}=0,10e,20e$).

The binding energy per atom is given by the difference between the tight-binding energy of a free carbon atom and its energy within the fullerene. Several interesting findings result from Fig. 11, where this quantity is plotted as a function of the excitation energy for selected total charges. Specifically, the negative drop occurring for relatively low excitation energies and high total charges accounts for the highly charged fullerenes lacking enough energy to dissociate, thus being unstable but remaining unfragmented. This low binding-energy region tends to vanish for energies and charges corresponding to increased fragmentation probability (see also Fig. 5). For total ionization states higher than $+5e$, with increasing excitation energy the binding energy shows successively a local minimum and a maximum. This behavior is best visible for $q_{\mathrm{tot}}=10e$ and, as expected, the excitation energy interval between the minimum and maximum corresponds precisely to the transition region in the fragmentation probability for the given total charge.

The fragment compactness may be expressed in terms of the average number of bonds formed within the fragments. For low-energy nonfragmenting trajectories, for which the fullerene cage is not distorted excessively, the number of bonds characterizing the C_{60} cage in equilibrium is preserved (90 bonds, each carbon atom having a threefold coordination). For each particular total ionization state bonds start breaking up for excitation energies above the fragmentation threshold. As one can see in Fig. 12, the decrease of the number of bonds is more pronounced with increasing total charge then with increasing excitation energy. For high ionization states the decrease is rather abrupt and roughly monotonous. By contrast, for neutral and low-charge fullerenes a discrete minimum followed by a maximum are noticeable in the transition region, indicating that during and immediately after the initial disintegration, fragments seem to recombine to a certain extent, producing incidentally compact structures. This leads to an increased average number of bonds, sometimes even exceeding the initial one. If sufficient excitation or electrostatic energy is transferred to the system, fragments become less compact and the number of bonds decreases significantly as dissociation progresses.

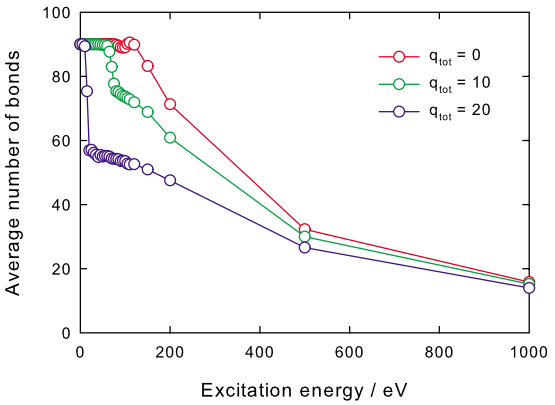

FIG. 12. (Color online) Average number of bonds as a function of the excitation energy for selected total charges ($q_{\mathrm{tot}}=0,10e,20e$).

It is easy to anticipate that a certain correlation does exist between the average binding energy and the average number of bonds. In Fig. 13 we have plotted both the charge-averaged correlation as a function of excitation energy and the excitation energy-averaged correlation as a function of the total charge. The dependences appear to be significant, exceeding the value 0.8 throughout. The charge-averaged correlation is lower for lower energies, since here, as noticeable from Figs. 11 and 12, the binding energy and the number of bonds appear to be particularly uncorrelated for higher charges. As mentioned when discussing the binding energy, the high-charge low-energy fragments are responsible for the instability of the system and, inherently, for fluctuations reducing the correlations. The excitation energy-averaged correlation shows a decrease for high charges, specifically around 19, for which the energy balance is dominated by the Coulomb interactions.

The size and charge distributions plotted in Figs. 3 and 4 offer an intuitive image on the fragmentation process, but provide no indication on the actual size-charge correlation. The contour plot in Fig. 14 illustrates precisely this correlation, offering a useful quantitative description. Superim-

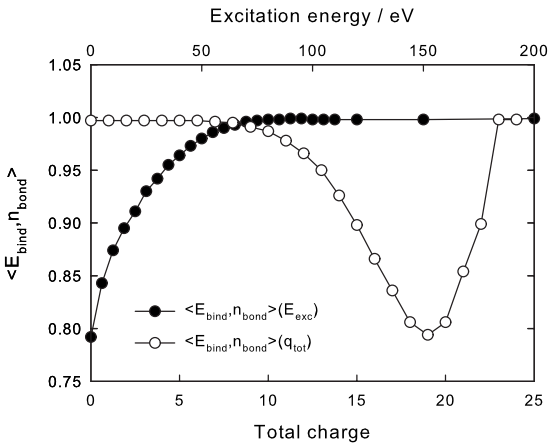

FIG. 13. Average binding energy-average number of bonds correlation as a function of total charge and excitation energy, respectively.

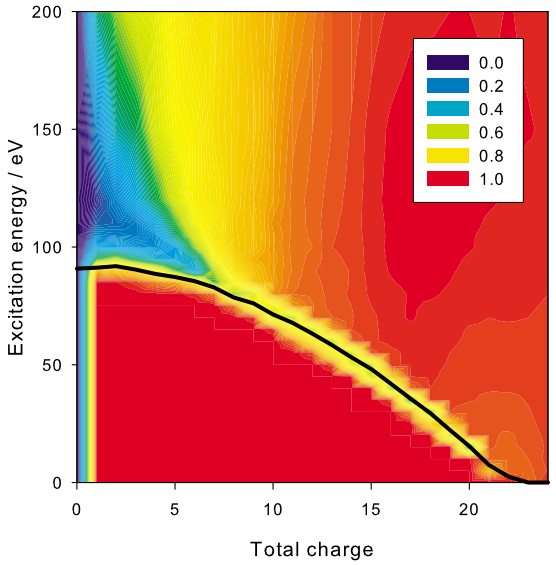

FIG. 14. (Color online) Critical excitation line (black) and contour plot of average size-average charge correlation as a function of total charge and excitation energy.

posed, the critical line (plotted in black) represents the fragmentation threshold, for which the probability amounts to 0.5, and delimits from the upper side the nonfragmenting region.

In the case of chargeless fragmentation, the correlation is evidently 0, while for charged fragments the correlation fluctuates between 1 and approximately 0.2. The highest correlation (represented with red) occurs inside the nonfragmentation region, where the whole charge resides on the unfragmented fullerene.

In the transition region, the correlation drops significantly, indicating the instability of the fragments. Qualitatively, the decrease in the correlation can be understood by recalling the relative shift noted between the average size and average charge distributions exemplified for the intermediate total charge $q_{\mathrm{tot}}=10e$ in Fig. 3. It appears that for moderate total charges the charge dynamics lags behind the fragmentation process, leading to overcharged fragments along with neutral ones.

For energies higher than the critical excitation energy but low-charge states ($\lesssim 5e$), the fragmentation proceeds with low size-charge correlation (bluish region in Fig. 14), since few charges are accommodated on many fragments and larger clusters are preferred such as to reduce the Coulomb repulsion.

It is hazardous to attempt to model the actual distribution of the overall ionization states in a particular fragmentation experiment, however, not departing from our idea to keep the model as simple as possible, but still catching the general features of the fragmentation experiments; the simplest assumption is that different total charge states occur with equal probability. Thus, by taking the average of the excitation energies along the critical line depicted in Fig. 14, one obtains approximately 55 eV. This value agrees well with the threshold of asymmetric dissociation (mainly caused by C_2 evaporation) found around 50 eV by Rentenier *et al.* in fragmentation experiments with $H^+_{x=1,3}$ (see Fig. 3 of Ref. 3).

IV. CONCLUSIONS

We present a detailed quantitative analysis of the radiation-induced fragmentation of the C_{60} fullerene performed using the tight-binding parametrization of Papaconstantopoulos *et al.*[29] embedded in MD simulations. A significant improvement over our previous approach,[25] with important implications on the results and their interpretation, arises from the explicit treatment of ionized fragments, nonadiabatic excitation, and charge-transfer processes. This approach improves significantly our results, which are in better agreement and allow for a more subtle understanding of the experimental findings than previous calculations.

We have considered systems excited up to 1000 eV and total ionization states up to $+24e$. The main quantities yielded by the simulations, namely, the fragment size and the fragment charge distributions, have been averaged over large ensembles of trajectories for each pair of total ionization state and excitation energy and have been used to derive several other quantities: average fragmentation probability, average number of fragments, average fragment size, and average fragment charges. Additionally, the average binding energy and the average number of bonds have been employed to characterize the stability and compactness of the resulted fragments. To address the interdependencies among different quantities, we have also examined correlation functions such as the size-charge correlation. For trajectories involving only neutral fragments the dissociation sets in around 80 eV, while for increasing total ionization states, the critical energy gradually decreases, such that for total charges exceeding $+23e$ fragmentation occurs without any additional energy supply.

A well-defined phase-transition region is found in the total charge-excitation energy plane, which appears to be delimited by a roughly parabolic critical line. The overall average critical excitation energy estimated from the simulations amounts to 55 eV and agrees fairly with the experimental findings of Rentenier *et al.*[3]

For moderate excitation energies (<150 eV) and intermediate total ionization states ($\leq 10e$), the fragment size profiles exhibit the typical experimentally observed U shape, as well as a bimodal dependence.[1,3,32–34] While for low energies, evaporation and cleavage of smaller clusters appear to be the prevalent mechanism, for high excitation energies multifragmentation turns out to be the main fragmentation channel. However, genuine power-law fragment distributions set in only beyond 1000 eV; monomers and dimers being predominantly observed for high excitation energies. Irrespective of the excitation energy, in highly ionized states the U-shape size distributions disappear, since the strong electrostatic repulsion between and within clusters produces further disintegration into smaller fragments.

The fragment charge distributions show qualitatively the same behavior as the fragment size distributions, however with a slight shift toward higher fragment sizes for moderate ionization states, implying a high probability of small *neutral* fragments to occur (mainly neutral C_2, by means of successive evaporations). Still, as clearly stated also by Boyle *et al.*,[11] we find that the C_3^{q+} loss is the dominant channel for high total ionization states and/or excitation energies, as revealed by the plots of the fragment distributions.

To account realistically for the finite durations of the laser pulses and the gradual charge buildup in typical experiments, we have devised a ramplike thermal excitation mechanism which also sets the total ionization state of the system. As expected, for a given input energy the instantaneous excitation is more effective (in terms of fragmentation probability and number of fragments) then finite ramp durations, which basically shift the fragmentation threshold to higher excitation energies. Whereas the total ionization state influences decisively the size/charge fragmentation profiles, by contrast, the actual details of a particular charge redistribution mechanism along the trajectory prove to be not crucial for high total charges.

The simulations have evidenced several interesting correlations between the measured quantities. For each given total charge and excitation energy, the product between the average fragment size (charge) and the average number of fragments is found to depart only within reasonably small statistical errors from the total number of atoms (total charge). Significant correlations (exceeding throughout 0.8) manifest themselves between the average binding energy and the average number of bonds, while more complicated correlations exist also between the average fragment size and charge, with pronounced lows tracking the instability regions in the total charge-excitation energy plane.

ACKNOWLEDGMENTS

The authors gratefully acknowledge the support by CNCSIS PN-II Grants No. 502 and 506.

*tbeu@phys.ubbcluj.ro

[1] E. B. Campbell and F. Rohmund, Rep. Prog. Phys. **63**, 1061 (2000).
[2] V. V. Afrosimov, A. A. Basalaev, M. N. Panov, and O. V. Smirnov, Fullerenes, Nanotubes, Carbon Nanostruct. **12**, 485 (2004).
[3] A. Rentenier, P. Moretto-Capelle, D. Bordenave-Montesquieu, and A. Bordenave-Montesquieu, J. Phys. B **38**, 789 (2005).
[4] D. M. Gruen, Nucl. Instrum. Methods Phys. Res. B **78**, 118 (1993).
[5] S. C. O'Brien, J. R. Heat, R. F. Curl, and R. E. Smalley, J. Chem. Phys. **88**, 220 (1988).
[6] E. E. B. Campbell, K. Hoffmann, H. Rottke, and I. V. Hertel, J. Chem. Phys. **114**, 1716 (2001).
[7] M. Tchaplyguine, K. Hoffmann, O. Duhr, H. Hohmann, G. Korn, H. Rottke, M. Wittmann, I. V. Hertel, and E. E. B. Campbell, J. Chem. Phys. **112**, 2781 (2000).
[8] I. Shchatsinin, T. Laarmann, G. Stibenz, G. Steinmeyer, A. Stal-

mashonak, N. Zhavoronkov, C. P. Schulz, and I. V. Hertelb, J. Chem. Phys. **125**, 194320 (2006).
[9] D. Bauer, F. Ceccherini, A. Macchi, and F. Cornolti, Phys. Rev. A **64**, 063203 (2001).
[10] S. Hunsche, T. Starczewski, A. l'Huillier, A. Persson, C. G. Wahlström, H. B. van Linden van den Heuvell, and S. Svanberg, Phys. Rev. Lett. **77**, 1966 (1996).
[11] M. Boyle, T. Laarmann, I. Shchatsinin, C. P. Schulz, and I. V. Hertel, J. Chem. Phys. **122**, 181103 (2005).
[12] T. Kobayashi, T. Kato, Y. Matsuo, M. Kurata-Nishimura, J. Kawai, and Y. Hayashizaki, J. Chem. Phys. **126**, 061101 (2007).
[13] B. Torralva, T. A. Niehaus, M. Elstner, S. Suhai, Th. Frauenheim, and R. E. Allen, Phys. Rev. B **64**, 153105 (2001).
[14] A. D. Boese and G. E. Scuseria, Chem. Phys. Lett. **294**, 233 (1998).
[15] Y. Ueno and S. Saito, Phys. Rev. B **77**, 085403 (2008).
[16] A. B. Young, L. M. Cousins, and A. G. Harrison, Rapid Commun. Mass Spectrom. **5**, 226 (1991).
[17] K. A. Caldwell, D. E. Giblin, C. S. Hsu, D. Cox, and M. L. Gross, J. Am. Chem. Soc. **113**, 8519 (1991).
[18] R. J. Doyle and M. M. Ross, J. Phys. Chem. **95**, 4954 (1991).
[19] M. C. Larsen, P. Hvelplund, M. O. Larsson, and H. Shen, Eur. Phys. J. D **5**, 283 (1999).
[20] K. Hansen, K. Hoffmann, and E. E. B. Campbell, J. Chem. Phys. **119**, 2513 (2003).
[21] T. A. Beu, J. Onoe, and K. Takeuchi, Eur. Phys. J. D **10**, 391 (2000).
[22] T. A. Beu, J. Onoe, and K. Takeuchi, Eur. Phys. J. D **17**, 205 (2001).
[23] T. A. Beu, J. Onoe, and A. Hida, Phys. Rev. B **72**, 155416 (2005).
[24] T. A. Beu and J. Onoe, Phys. Rev. B **74**, 195426 (2006).
[25] L. Horvath and T. A. Beu, Phys. Rev. B **77**, 075102 (2008).
[26] E. Kim, Y. H. Lee, and J. Y. Lee, Phys. Rev. B **48**, 18230 (1993).
[27] S. G. Kim and D. Tomanek, Phys. Rev. Lett. **72**, 2418 (1994).
[28] Q. M. Zhang, J.-Y. Yi, and J. Bernholc, Phys. Rev. Lett. **66**, 2633 (1991).
[29] D. A. Papaconstantopoulos, M. J. Mehl, S. C. Erwin, and M. R. Pederson, in *Tight-Binding Approach to Computational Materials Science*, edited by P.E.A. Turchi, A. Gonis, and L. Colombo, MRS Symposia Proceedings No. 491 (Materials Research Society, Pittsburgh, 1998), p. 221.
[30] C. S. Yannoni, P. P. Bernier, D. S. Bethune, G. Meijer, and J. R. Salem, J. Am. Chem. Soc. **113**, 3190 (1991).
[31] R. K. Kremer, Appl. Phys. A: Solids Surf. **56**, 211 (1993).
[32] A. Itoh, H. Tsuchida, K. Miyabe, T. Majima, and Y. Nakai, Phys. Rev. A **64**, 032702 (2001).
[33] A. Itoh and H. Tsuchida, Nucl. Instrum. Methods Phys. Res. B **195**, 216 (2002).
[34] R. Ehlich, M. Westerburg, and E. E. B. Campbell, J. Chem. Phys. **104**, 1900 (1996).
[35] T. Schlathölter, R. Hoekstra, and R. Morgenstern, J. Phys. B **31**, 1321 (1998).
[36] T. LeBrun, H. G. Berry, S. Cheng, R. W. Dunford, H. Esbensen, D. S. Gemmell, E. P. Kanter, and W. Bauer, Phys. Rev. Lett. **72**, 3965 (1994).